Perovzalates: a family of perovskite-related oxalates

Rebecca Clulow[1], Alasdair Bradford[1,2], Stephen L. Lee[2] and Philip Lightfoot[1*]

1. School of Chemistry and EaStChem, University of St Andrews, St Andrews, Fife, KY16 9ST, UK
2. School of Physics, University of St Andrews, St Andrews, Fife, KY16 9SS, UK

*E-mail: pl@st-andrews.ac.uk

Abstract

A family of hybrid ***Perov***skite-o***xalates*** ("Perovzalates") of general composition $A^{I}Li_3M^{II}(C_2O_4)_3$ (A = K^+, Rb^+, Cs^+; M = Fe^{2+}, Co^{2+}, Ni^{2+}) are presented. All eight new compounds are isostructural with the previously reported examples $NH_4Li_3Fe(C_2O_4)_3$ and $KLi_3Fe(C_2O_4)_3$, crystallising in the rhombohedral space group $R\bar{3}c$, with *a* ~11.3 - 11.6 Å, *c* ~14.8 – 15.2 Å. In contrast to other families of "hybrid perovskites" such as the formates, these compounds can be regarded as closer structural relatives to inorganic (oxide) perovskites, in the sense that they contain direct linkages of the octahedral sites *via* bridging oxygen atoms (of the oxalate groups). It is of note, therefore, that monoatomic cations as large as Cs^+ can be incorporated into the perovskite-like A sites this structures type, which is not feasible in traditional ABO_3 perovskites; indeed $CsLi_3Ni(C_2O_4)_3$ appears to exhibit the 'mostly tightly bound' 12-coordinate Cs^+ ion in an oxide environment, according to a bond valence analysis.

Introduction

Perovskites (general formula ABX_3) have dominated the field of functional materials and exhibit a wide range of properties including superconductivity, ferroelectricity and magnetism.[1] The introduction of organic components into the traditional perovskite structure could improve both the toxicity and sustainability of the compounds and introduce greater structural diversity. Hybrid perovskites, which may contain organic moieties at either the A, B or X sites, or further combinations of these, are already a highly-studied group of materials and there are many examples of such compounds with interesting properties.[2,3] Examples of complex anions that may be incorporated at the perovskite-like X site are cyanide, formate, azide, tetrahydroborate and hypophosphite.[4–7] Whilst the oxalate ligand is already extensively used in coordination polymers, its ability to form perovskite-like structures has only recently been recognised in the composition $KLi_3Fe(C_2O_4)_3$.[8] Here, we extend our studies of this unusual structure type by showing that substitution of K by Rb or Cs and of Fe by Co or Ni is feasible. Hence, eight new compositions, $A^{I}Li_3M^{II}(C_2O_4)_3$ (A = K^+, Rb^+, Cs^+; M = Fe^{2+}, Co^{2+}, Ni^{2+}), are reported and their structural variations are discussed.

Experimental

Crystalline samples were synthesised *via* a hydrothermal method from commercially available reagents. The reactions mixtures were heated between 160 and 220 ˚C in a Teflon lined autoclave for 3 to 6 days. The resultant products were subsequently filtered and dried overnight at 50 ˚C prior to analysis by X-ray diffraction. Reactions typically produced a mixture of phases, and several variants of

composition/temperature/solvent were explored to increase yield and purity. Further synthetic details are provide in ESI. Nevertheless, suitable single crystals could be isolated using an optical microscope and X-ray diffraction data were collected on a Rigaku SCXmini desktop instrument using Mo Kα_1 radiation (λ = 0.7107 Å) at 173 K. The data were processed using Rigaku CrystalClear software and were solved and refined using the SHELX package within the WINGX program.[9–11] Powder X-ray diffraction data were collected on a PANalytical Empyrean diffractometer using Cu Kα_1 radiation (λ = 1.5406 Å) at ambient temperature. The data were collected between 5 - 70˚ for one hour, and subsequently analysed using the Rietveld method using GSAS and the Expgui interface.[12,13] Magnetic data were collected on a quantum design MPMS SQUID instrument between 300 K and 2 K. Data were collected at zero field and at 100 Oe at 10 K intervals between 300 and 20 K and 2 K increments between 20 K and 2 K. Samples initially underwent a zero field cool (ZFC) followed by a field heating/cooling cycle (FC).

Results and discussion

All eight new compositions crystallise in the same structure type, isotypic with $KLi_3Fe(C_2O_4)_3$,[8] in space group $R\,\bar{3}\,c$ (Table 1). In fact, the first compound reported with this structure type was $NH_4Li_3Fe(C_2O_4)_3$,[14] but the relationship to the perovskite structure was not noted in that work. The direct relationship to the "cubic" ABX_3 perovskite structure can be most clearly seen if the carbon atoms of the oxalate moiety are regarded as secondary features, both in the stoichiometry of the compound and in the corresponding structural description. Thus, Figure 1 shows the octahedral framework of an idealised cubic perovskite, compared to the corresponding framework in the perovzalate family. The stoichiometry of perovzalate may be written $[A^{I}(vac)_3]_A[Li_3M^{II}]_B[C_6O_{12}]_X$ to emphasise the simultaneous 1:3 ordering of A^{I}/vacancies at the A-site and M^{II}/Li at the B-site in an idealised "$A_4B_4X_{12}$" quadruple perovskite.

Table 1 Crystallographic data and refinement details

Formula	$KLi_3Co(C_2O_4)_3$	$KLi_3Ni(C_2O_4)_3$	$RbLi_3Fe(C_2O_4)_3$	$RbLi_3Co(C_2O_4)_3$	$RbLi_3Ni(C_2O_4)_3$	$CsLi_3Fe(C_2O_4)_3$	$CsLi_3Co(C_2O_4)_3$	$CsLi_3Ni(C_2O_4)_3$
Formula Weight	382.91	382.69	426.20	429.28	429.06	473.64	476.72	476.50
Density (g cm^{-3})	2.277	2.304	2.465	2.515	2.542	2.666	2.713	2.740
Crystal System	Trigonal	Trigonal	Trigonal	Trigonal	Trigonal	Trigonal	Trigonal	Trigonal
Space Group	$R\bar{3}c$	$R\bar{3}c$	$R\bar{3}c$	$R\bar{3}c$	$R\bar{3}c$	$R\bar{3}c$	$R\bar{3}c$	$R\bar{3}c$
a/Å	11.3215(9)	11.3071(8)	11.4780(8)	11.4019(8)	11.3796(7)	11.6046(8)	11.5264(8)	11.4908(8)
b/Å	11.3215(9)	11.3071(8)	11.4780(8)	11.4019(8)	11.3796(7)	11.6046(8)	11.5264(8)	11.4908(8)
c/Å	15.0942(13)	14.9434(12)	15.1001(12)	15.1029(12)	14.9962(10)	15.1779(12)	15.2164(1)	15.1534(10)
α(˚)	90	90	90	90	90	90	90	90
β(˚)	90	90	90	90	90	90	90	90
γ(˚)	120	120	120	120	120	120	120	120
V/$Å^3$	1675.5(3)	1654.6(3)	1722.8(3)	1700.4(3)	1681.8(2)	1770.1(3)	1750.8(3)	1732.8(3)
Z	6	6	6	6	6	6	6	6
Measured Ref	5415	5246	5535	5449	5226	5297	5481	5412
Independent Ref	436 [R(int) = 0.1083]	426 [R(int) = 0.0432]	446 [R(int) = 0.0542]	444 [R(int) = 0.0803]	441 [R(int) = 0.0747]	447 [R(int) = 0.0994]	444 [R(int) = 0.0439]	442 [R(int) = 0.0384]
Refined Parameter	37	37	37	37	37	37	37	27
GOOF	0.631	0.711	0.815	0.610	0.876	1.145	0.853	0.935
Final R Indices (I > 2σ(I))	R1 = 0.0329, wR2 = 0.0808	R1 = 0.0216, wR2 = 0.0748	R1 = 0.0251, wR2 = 0.0886	R1 = 0.0274, wR2 = 0.0736	R1 = 0.0328, wR2 = 0.1025	R1 = 0.0346, wR2 = 0.1153	R1 = 0.0202, wR2 = 0.0920	R1 = 0.0229, wR2 = 0.1012

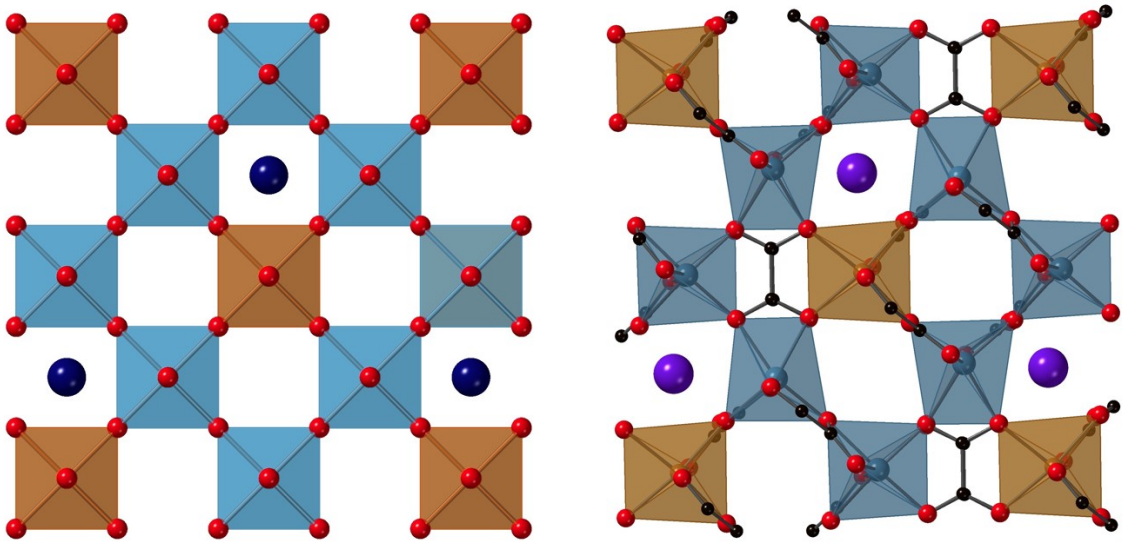

Figure 1. Hypothetical "cubic" perovskite structure incorporating simultaneous 1:3 cation ordering at both the B and A sites (left) and the corresponding observed perovzalate structure (right). LiO_6 octahedral are shaded blue, $M^{II}O_6$ octahedra brown and A^{I} cations purple. Note that there are direct B-O-B links mediated *via* the oxalate groups.

The particular arrangement of simultaneous 1:3 cation ordering at both the A and B perovskite sites has no precedent in traditional perovskite chemistry.[15] The closest examples are the $CaCu_3Ti_4O_{12}$ structure type,[16] having 1:3 A-site ordering and derivatives such as $CaCu_3Fe_2Sb_2O_{12}$, which also has 1:1 B-site order.[17] Further insight into the nature of this ordering pattern can be gleaned from examining the local coordination around each of the crystallographically-distinct A-sites. Figure 2 compares the generic cubic perovskite unit cell, with A at the body-centre position, B at the cell corners and X at each cell edge, with the corresponding pseudo-cubes in perovzalate. It can be seen that there are two distinct types of "cube" in perovzalate. In common with perovskite itself, both are surrounded by eight corner-shared BO_6 octahedra, with two of the B-sites being occupied by M^{II} (across a body-diagonal), but whereas those with A^{I} at the centre have a fairly conventional environment, the ones with vacancies at the centre are "capped" across two opposite cube faces by oxalate moieties. This feature itself is obviously incompatible with occupancy of these particular cubes by any typical A-site cation, as it would lead to unfavourable A-carbon contacts. This drives the specific 1:3 ordering observed. The asymmetric unit contains one of each cation type, each on a special position in space group $R\bar{3}c$ (hexagonal setting) with Wyckoff positions/site symmetries: A^{I} (6b, $\bar{3}$); M^{II} (6a, 32); Li (18e, .2). Resulting bond lengths, angles and bond valence sums (BVS)[18] for each composition are given in Table 2. The local coordination environments around the A^{I} and M^{II} sites are shown in Figure 3.

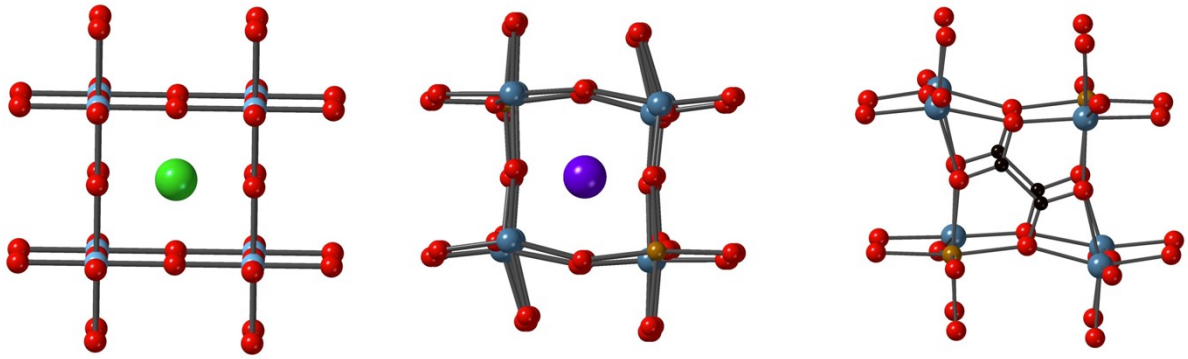

(a) (b) (c)

Figure 2. Comparison of perovskite A sites (a) cubic $SrTiO_3$, (b) A site of $A^{I}Li_3M^{II}(C_2O_4)_3$ and (c) vacant site of $A^{I}Li_3M^{II}(C_2O_4)_3$, *trans*-capped by oxalate groups.

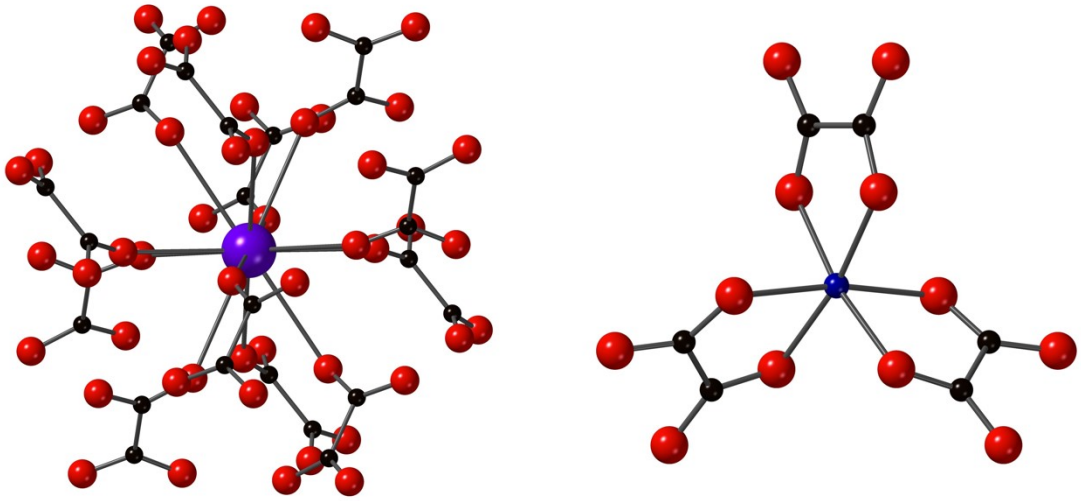

Figure 3. Local coordination environments of A^{I} (left) and M^{II} (right) of perovzalate $A^{I}Li_3M^{II}(C_2O_4)_3$. A^{I} cations are purple, M^{II} cations blue, oxygen atoms red and carbon atoms black.

Naturally, as the absolute and relative sizes of the three cationic species varies, structural distortions are also influenced. The Li coordination environment, however, changes little across the series, and its bond valence is close to ideal. The varying size of the M^{II} site results in systematically reduced 'bite' angles for the oxalate ligand versus increasing M^{II} size, for each series, A^{I} = K, Rb, Cs (Figure 4). This results in more "distorted" MO_6 octahedra, as quantified by a conventional distortion index, δ^2, $\delta^2 = \frac{1}{11}\sum(\theta_i - 90)^2$ (Table 3), although the LiO_6 octahedra are significantly more distorted in each case. The most dramatic, and perhaps surprising, structural effect, however, is in the nature of bonding at the A^{I} sites. Taking each as 12-coordinate, the bond valence sum at A^{I} increases dramatically with ionic size, such that Cs^{+} has BVS values far in excess of those normally observed. In each case, the mean Cs-O bond length is well below that found in the comprehensive study of Gagné[19] (mean Cs^{XII}-O = 3.377 Å). Gagné quotes a minimum mean bond length of 3.207 Å for Cs^{XII}-O whereas the mean Cs-O bond length in $CsLi_3Ni(C_2O_4)_3$ is only 3.155 Å, and the corresponding BVS of Cs in $CsLi_3Ni(C_2O_4)_3$ is 1.44 valence units (v.u.) using Gagné's revised bond valence parameters for Cs^{XII}-O[19], and as high as 1.64 v.u. using Brese's parameters[18]. Indeed Gagné's full list of compounds containing CsO_{12} polyhedra contains only five compounds with their six shortest Cs-O bond of the order of ~3.12

Å or lower. Most of these have their next six Cs-O bonds considerably longer. Of note are the compounds $Cs_2PbCu(NO_2)_6$[20] and $CsNa_3Li_{12}(GeO_4)_4$,[21] which appear to have the highest BVS for CsO_{12} environments amongst previously reported, well-determined structures: *viz*., 1.32 and 1.35 v.u., respectively, using Gagné's BV parameters. Other Cs oxalates, for example $CsHC_2O_4$[22] (BVS for Cs^{XII}-O = 1.13 v.u.), do not show such extreme over-bonding of Cs. A fuller list of calculated Cs BVS values from Gagné's list is provided in ESI.

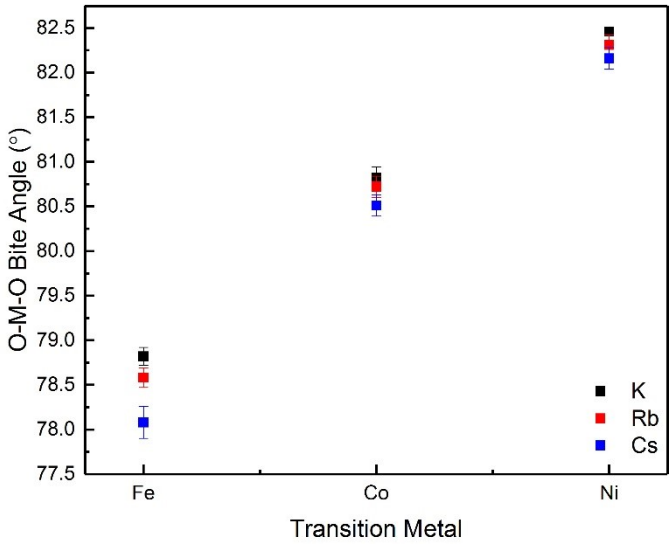

Figure 4. Variation of O-M-O bite angles (˚) of perovzalates ($A^{I}Li_3M^{II}(C_2O_4)_3$) with A^{I} and M^{II} cations

Table 3. Distortion parameters, δ^2, for the Li and M sites in ($A^{I}Li_3M^{II}(C_2O_4)_3$)

Alkali Metal		$ALi_3Fe(C_2O_4)_3$	$ALi_3Co(C_2O_4)_3$	$ALi_3Ni(C_2O_4)_3$
K	M^{II}	47.94	32.63	21.24
	Li	196.8	195.1	194.1
Rb	M^{II}	49.44	32.64	22.16
	Li	206.1	202.2	202.4
Cs	M^{II}	54.41	33.99	23.83
	Li	222.7	218.3	218.0

An additional measure of the bonding at the A and B sites in perovskites is the tolerance factor (*t*). These are shown for the present family in Table 4 (calculated using Shannon's ionic radii[23] for 12-ccordinate A^{I} and 6-coordinate Li, M^{II}, O^{2-}) . As can be seen, the potassium-containing members of this family fall within the reasonably allowed tolerance factor limits seen in conventional oxides perovskites, whereas the Rb and Cs derivatives lie well above the ideal value of t = 1. In the case of conventional oxide perovskites the "cubic" perovskite structure would be unstable for such high t values, and preferential formation of a hexagonal perovskite or other structure type would occur. Apparently in this family the perovskite-like octahedral framework is further stabilised by the additional influence of the bridging oxalate moieties, despite the compressive strain at the large A-site cations. We note that there are no examples of significant Rb or Cs incorporation into cubic ABO_3 perovskites, whereas such structures do exist for the corresponding fluorides, where the divalent (i.e. relatively large) cation on the B-site permits the incorporation of a larger A-site cation. Thus, $CsCaF_3$ (t = 0.98) adopts the cubic perovskite structure, whereas $CsNiF_3$ (t = 1.13) adopts a hexagonal (2H)

perovskite structure. Cs^+ represents the largest available monatomic cation. In order to "push" the geometric limits of the present structure type we attempted reactions aimed at preparing analogues with larger (e.g. methylammonium) or smaller (Na^+) cations at the A-site. So far, this has been unsuccessful, suggesting a stability region incorporating only K, Rb or Cs at the A-site in the perovzalate family.

Table 4. Tolerance factors of the perovzalate compounds ($A^{I}Li_3M^{II}(C_2O_4)_3$)

Alkali Metal	$ALi_3Fe(C_2O_4)_3$	$ALi_3Co(C_2O_4)_3$	$ALi_3Ni(C_2O_4)_3$
K	1.000	1.004	1.010
Rb	1.026	1.031	1.037
Cs	1.080	1.084	1.091

Preliminary magnetic measurements were carried out on several samples that exhibited good phase purity. The $1/\chi$ versus T data for two samples are shown in Figure 5, with a linear Curie-Weiss fit in the region 150 – 300 K. Both samples show no evidence of magnetic ordering down to 2 K, perhaps not surprising for such magnetically-dilute systems. Derived parameters for $KLi_3Co(C_2O_4)_3$ and $KLi_3Ni(C_2O_4)_3$, respectively are θ = -2.00 K, -25.0 K; C = 2.899 $cm^3\ mol^{-1}$, C = 1.635 $cm^3\ mol^{-1}$; μ_{eff} = 4.815 μ_B, 3.62 μ_B, both of which are within the expected range for the high-spin divalent cations.[24]

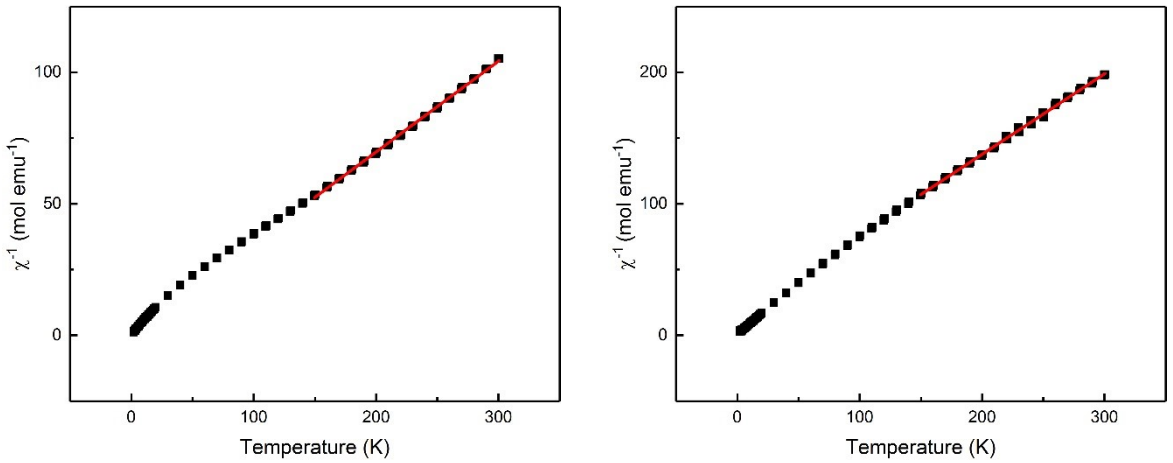

Figure 5. Magnetisation data (1/χ versus T) for (left) $KLi_3Co(C_2O_4)_3$ and (right) $KLi_3Ni(C_2O_4)_3$

Table 2 Bond lengths (Å) and bond valence sums (valence units)[18] derived from single crystal data collected at 173 K

	$KLi_3Co(C_2O_4)_3$	$KLi_3Ni(C_2O_4)_3$	$RbLi_3Fe(C_2O_4)_3$	$RbLi_3Co(C_2O_4)_3$	$RbLi_3Ni(C_2O_4)_3$	$CsLi_3Fe(C_2O_4)_3$	$CsLi_3Co(C_2O_4)_3$	$CsLi_3Ni(C_2O_4)_3$
Li-O	2.019(6) × 2	2.020(3) × 2	2.024(6) × 2	2.029(7) × 2	2.023(6) × 2	2.032(7) × 2	2.038(5) × 2	2.042(5) × 2
	2.130(3) × 2	2.1344(14) × 2	2.138(3) × 2	2.147(3) × 2	2.161(3) × 2	2.177(4) × 2	2.185(3) × 2	2.197(3) × 2
	2.165(6) × 2	2.152(3) × 2	2.196(6) × 2	2.178(6) × 2	2.174(5) × 2	2.230(7) × 2	2.215(5) × 2	2.203(5) × 2
BVS	1.08	1.09	1.05	1.05	1.04	0.98	0.98	0.97
M-O	2.083(2) × 6	2.0523(10) × 6	2.127(2) × 6	2.089(2) × 6	2.053(2) × 6	2.132(3) × 6	2.095(2) × 6	2.059(2) × 6
BVS	2.09	2.16	2.07	2.05	2.16	2.05	2.02	2.13
K-O	3.007(2) ×6	3.0179(9) × 6	3.057(2) × 6	3.048(2) × 6	3.0560(17) × 6	3.1228(19) × 6	3.1199(15) × 6	3.1240(17) × 6
	3.152(2) × 6	3.1215(11) × 6	3.193(2) × 6	3.164(2) × 6	3.139(2) × 6	3.234(4) × 6	3.207(2) × 6	3.186(2) × 6
BVS	0.94	0.96	1.19	1.24	1.27	1.55	1.61	1.64

Conclusions

We have presented a family of hybrid perovskite-related oxalates ("Perovzalates") of general composition $A^{I}Li_3M^{II}(C_2O_4)_3$ ($A = K^+, Rb^+, Cs^+$; $M = Fe^{2+}, Co^{2+}, Ni^{2+}$). All compounds are isostructural, with rhombohedral symmetry, and can be regarded as derived from the traditional oxide perovskite structure, ABO_3, by replacement of oxide ligands by oxalate groups with concomitant ordering of K^+/vacancies at the A site and Li/M^{II} at the B-site. The ordering correlates with accommodation of the oxalate groups, which effectively "cap" the opposite faces of unoccupied A-site cubes. A particularly unusual feature of this family is that cations as large as Cs^+ can be accommodated at the perovskite-like A-site; a phenomenon which has not been seen in traditional oxide perovskites. In fact, existing data suggest that $CsLi_3Ni(C_2O_4)_3$ sets a "world record" for the most tightly bound 12-coordinate caesium atom in an oxide environment.

Acknowledgements

We would like to thank the University of St Andrews, and the EPSRC (doctoral studentship to RC: DTG012 EP/K503162-1) for funding.

Supporting information: synthesis details, powder XRD data and bond valence analyses.
Single crystal X-ray diffraction data for all refinements have been deposited: CDS deposition numbers 1944088-1944095
The research data pertaining to this paper are available at
https://doi.org/10.17630/74dd1b0a-1ed2-4d93-aeb0-128182fe7bed

References

1 J. P. Attfield, P. Lightfoot and R. E. Morris, *Dalton Trans.*, 2015, **44**, 10541–10542.
2 B. Saparov and D. B. Mitzi, *Chem. Rev.*, 2016, **116**, 4558–4596.
3 P. Jain, V. Ramachandran, R. J. Clark, D. Z. Hai, B. H. Toby, N. S. Dalal, H. W. Kroto and A. K. Cheetham, *J. Am. Chem. Soc.*, 2009, **131**, 13625–13627.
4 G. Kieslich and A. L. Goodwin, *Mater. Horizons*, 2017, **4**, 362–366.
5 X. Y. Wang, L. Gan, S. W. Zhang and S. Gao, *Inorg. Chem.*, 2004, **43**, 4615–4625.
6 M. Trzebiatowska, M. Maczka, M. Ptak, L. Giriunas, S. Balciunas, M. Simenas, D. Klose and J. Banys, *J. Phys. Chem. C*, 2019, **123**, 11840–11849.
7 Y. Wu, T. Binford, J. A. Hill, S. Shaker, J. Wang and A. K. Cheetham, *Chem. Commun.*, 2018, **54**, 3751–3754.
8 W. Yao, Y.Y. Guo and P. Lightfoot, *Dalton Trans.*, 2017, **46**, 13349–13351.
9 Rigaku, CrystalClear. Rigaku Corporation, Tokyo, Japan, 2014.
10 G. M. Sheldrick, *Acta Crystallogr. Sect. C Struct. Chem.*, 2015, **71**, 3–8.
11 L. J. Farrugia, *J. Appl. Crystallogr.*, 2012, **45**, 849–854.
12 A. C. Larson and R. B. Von Dreele, *General Structure Analysis System (GSAS)*, 2004.
13 B. H. Toby, *J. Appl. Crystallogr.*, 2012, **34**, 210-213.
14 J. H. Li, H. Liu, L. Wei and G. M. Wang, *Solid State Sci.*, 2015, **48**, 225–229.
15 M. V. Talanov, *Acta Crystallogr. Sect. A*, 2019, **75**, 379–397.

16 A. Deschanvres, B. Raveau and F. Tollemer, *Bull. Chim. Soc. Fr*, 1967, **11**, 4077–4078.
17 W. T. Chen, M. Mizumaki, T. Saito and Y. Shimakawa, *Dalt. Trans.*, 2013, **42**, 10116–10120.
18 N. E. Brese and M. O'Keeffe, *Acta Crystallogr. Sect. B*, 1991, **47**, 192–197.
19 O. C. Gagné and F. C. Hawthorne, *Acta Crystallogr. Sect. B Struct. Sci. Cryst. Eng. Mater.*, 2016, **72**, 602–625.
20 H. Ahsbahs, H. Sowa and E. Hellner, *Fortschritte der Mineral. Beih.*, 1982, **60**, 35–36.
21 R. Brandes and R. Hoppe, *Z. anorg. allg. Chem.*, 1995, **621**, 713–718.
22 L. N. Kholodkovskaya, V. K. Trunov and N. B. Tskhelashvili, *J. Struct. Chem.*, 1990, **31**, 667–670.
23 R. D. Shannon, *Acta Crystallogr. Sect. A*, 1976, **32**, 751-767.
24 F. A. Cotton and G. Wilkinson, *Advanced Inorganic Chemistry: A Comprehensive Text*, John Wiley & Sons Ltd., New York, 4th edn., 1980.